

# Synthesis, photophysical properties and catalytic activity of K<sup>3</sup>-SCS pincer palladium (II) complex of N,N'-di-tert-butylbenzene-1,3-dicarbothioamide supported by DFT analysis

Debasish Das<sup>a,f,\*</sup>, S. Kannan<sup>b,f</sup>, Mukesh Kumar<sup>c,f</sup>, Biswajit Sadhu<sup>d</sup>, Liladhar B. Kumbhare<sup>e</sup>

<sup>a</sup>Waste Management Division, Bhabha Atomic Research Centre, Mumbai 400085, India

<sup>b</sup>Fuel Chemistry Division, Bhabha Atomic Research Centre, Mumbai 400085, India

<sup>c</sup>Radiation Biology & Health Sciences Division, Bhabha Atomic Research Centre, Mumbai 400085, India

<sup>d</sup>Health Physics Division, Bhabha Atomic Research Centre, Mumbai 400085, India

<sup>e</sup>Chemistry Division, Bhabha Atomic Research Centre, Mumbai 400085, India

<sup>f</sup>Homi Bhabha National Institute, Anushaktinagar, Mumbai 400094, India

\*Corresponding author.

Email address: deba.chem@gmail.com, debads@barc.gov.in (Debasish Das)

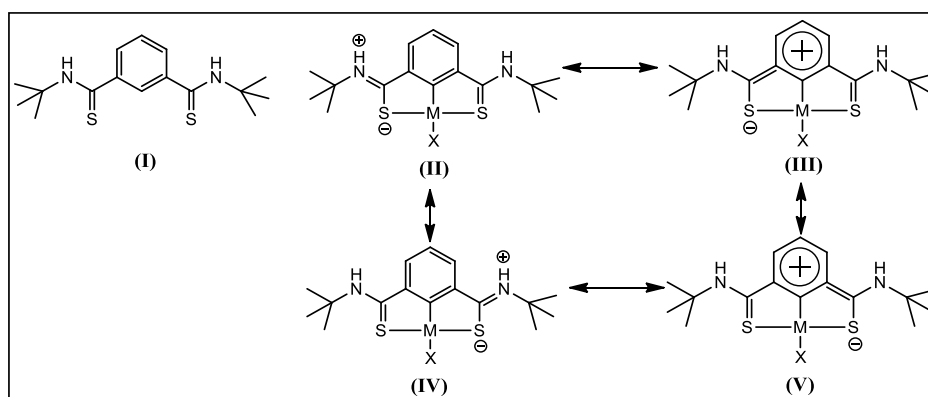
## Abstract

The title complex [PdCl(L)] (**1**), is obtained from the reaction of SCS pincer ligand HL (where, HL = N,N'-di-tert-butylbenzene-1,3-dicarbothioamide) with lithium tetrachloropalladate (II) in methanol. The compound **1** is characterized by elemental analysis, FTIR, <sup>1</sup>H, and <sup>13</sup>C-NMR spectroscopy, UV-Vis spectroscopy, powder X-ray diffraction and X-ray crystallographic techniques. At room temperature, **1** emits luminescence light of wavelength 460 nm in the solid state upon excitation by UV light of wavelength 280 nm. The average emission lifetime indicates that, both the ligand and complex emission is fluorescence in nature and involves mainly ligand centers  $\pi$ - $\pi^*$  deexcitation. It also shows good catalytic activity towards Mizoroki-Heck and Suzuki-Miyaura cross-coupling reactions of aryl bromides with tert-butyl acrylate and p-tolylboronic acid respectively. For both type of reactions, more than 99% conversion of the substrates is found to occur for electronically activated p-nitro bromobenzene using 1 mol % of **1**. Further, modern DFT calculations are performed to decipher the mechanistic insight on the preferable pathways of the Mizoroki-Heck cross-coupling reaction. Stepwise free energy of reactions for various probable reaction pathways suggest that the catalytic route has profound preference for Pd(0)-Pd(II) over Pd(II)-Pd(IV) pathway.

**Keywords:** Palladium, pincer complex, X-ray crystallography, luminescence, organometallic compound

## 1. Introduction

Palladium pincer complexes are well known for their excellent catalytic activity and some of them exhibit good photoluminescence in the glassy frozen state condition and even at room temperature [1-3]. The structural and bonding properties of these complexes vary significantly with slight modification of the functional group and skeleton of the bonded ligand. In some thiocarboxamide based complexes, one of the  $\alpha$ -carbon atoms to the amide takes part in the bonding with the metal atoms rather than the ortho-carbon of the aromatic ring [4,5]. It has also been observed that, the reaction conditions (temperature, solvent etc.) render a significant influence on the type of complex formed and metal-ligand stoichiometry [4,6]. Extensive studies have been carried out on several pincer ligands with various combinations of C, N, S and P donors and related palladium/platinum complexes have been investigated for their photophysical and catalytic properties [7-12]. Amongst the well-known pincer complexes, the thioamide based ligands with SCS type are relatively less explored compared to the others [13,14]. Therefore, in order to examine the binding properties and associated photophysical and catalytic properties of these complexes, one of the methyl groups of each side of N,N,N',N'-tert methylbenzene 1,3-dicarbothioamide are replaced by bulky tert-butyl group and another by hydrogen atom and employed for the complexation with Pd(II). It is worth mentioning that, thiocarbamide group bearing NH moiety can promote amino-thione and imino-thiol tautomerism and modulate the electron density on the central metal atom as is shown in scheme 1. The ligand can act as mono and dianionic ligand depending on the nature of solvent, central backbone and base added into the medium [15]. Moreover, the protonation-deprotonation of the secondary thioamide group and the hydrogen bonding between NH and any H-bond acceptor have a profound effect on the structure, properties as well as reactivities of the related complexes [16-18].



**Scheme 1.** Different canonical structures of free and bound ligand

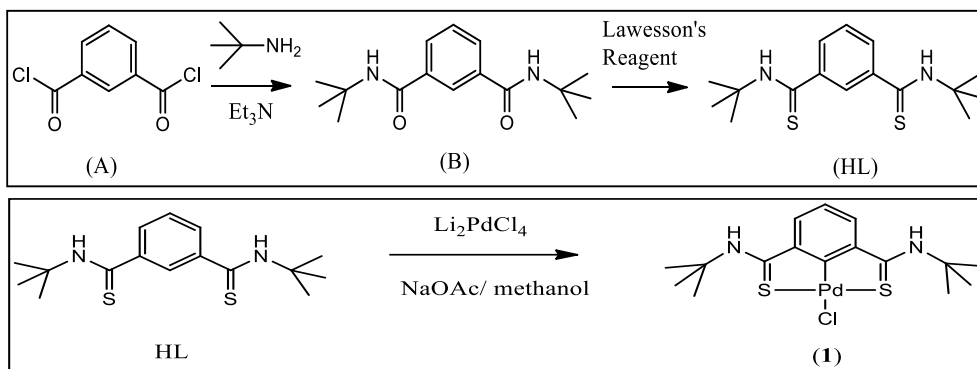
At low temperature, these types of complexes generally show intense emissions in the solid state [19, 20] but room-temperature luminescence particularly that of mononuclear Pd(II) complexes are scarcely found [2]. Sometimes these complexes show superior photoluminescence properties in solid state either in form of crystal or powder than in solution due to aggregation-induced emission. Further, it is found that, the emission intensity can be increased many folds by incorporating these in suitable polymer matrix. It is due to the increase in structural rigidity through chemical attachment of the co-ligand with the polymer by hydrogen bonding. This is expected for secondary thioamide based complexes rather than tertiary thioamide based complexes [21]. Therefore, it is essential to investigate the relationship between their structure and photophysical properties so that their utilization as optical devices could be fulfilled. Apart from that, the pincer types of complexes have shown great promise as catalyst for the Suzuki-Miyaura and Mizoroki-Heck cross-coupling reactions [18,22,23]. These reactions enable us to have direct carbon-carbon bond formation in the aromatic system under mild conditions. In this way, the complexes can be utilized in applications towards the synthesis of pure materials via environmental friendly route [24-26].

Although many thioamide based ligands and their pincer complexes with palladium and platinum have been previously reported along with their photophysical and catalytic properties, but systematic and combined study on the synthesis, luminescence properties with TD-DFT analysis for evaluation of electronic transition, and catalytic performance with DFT analysis to determine the actual reaction pathway are a handful in literature. Herein, we have performed these studies together with additional investigation on the probable generation route of elemental Pd from the pre-catalyst **1** in the reaction medium. This indicates that, decoordination of one of the thioamide group is essential before the actual reduction of Pd(II) to elemental Pd.

## 2. Results and discussion

### 2.1. Synthesis and spectroscopic analysis

The carboxamide, *N,N'*-ditertiarybutyl 1,3-benzenedicarboxamide is reacted with Lawesson's reagent in similar manner [27], which produced HL (Scheme 2 top) with yield more than 85%. The GC-MS spectrum of HL shows the presence of molecular ion peak at 308 (*m/z*) (Fig. S1). The reaction of HL with  $\text{Li}_2\text{PdCl}_4$  in presence of sodium acetate in methanol yielded the pincer complex  $[\text{PdCl}(\text{L})]$  (**1**) (Scheme 2 bottom), similar to the previous reports [20]. In contrast to HL, *N,N'*-ditertiarybutyl 1,3-benzenedicarboxamide failed to yield the corresponding pincer complex even after refluxing for 10 h. It suggests that, the coordination of soft S-atoms of thioamide groups facilitates ortho,ortho-cyclometallation with soft Pd(II) to form **1**. The IR spectrum shows that the stretching frequency of C(S)–N bond in **1** is  $16\text{ cm}^{-1}$  more than in HL (Fig. S2-S3). The similar increment of C–N stretching frequency due to cyclopalladation was also observed in the previously reported studies [6]. It clearly indicates that the thioamide group is coordinated directly to the Pd(II) center through S atoms and resulted in strengthening the C–N bond of the ligand through the formation of partial double bond between carbamoyl C and N-atoms. The different canonical structures of the ligand HL in free and bound conditions with the metal ion are presented in the Scheme 1. It can be clearly seen that structures II and IV show partial double bond character for C(S)–N bond and it is responsible for the increase in stretching frequency of the C–N bond as observed in the IR spectrum of the complex [13,15]. The  $^1\text{H}$  and  $^{13}\text{C}$ - NMR data of HL and **1** are as expected from their molecular structure. All protons of both *N*-<sup>t</sup>Bu groups of the ligand in combination show a single singlet peak in original as well as in the complex (Fig. S4-S5). Relative peak integration of aromatic protons in  $^1\text{H}$  NMR spectra of ligand and complex indicates that the number of phenyl ring protons in the complex is one less than the free ligand due to deprotonation at C-2 position as a result of formation of symmetric complex **1** (Fig. S5). The signals of NH protons of the ligand are strongly deshielded upon complexation ( $\Delta\delta = 2.03\text{ ppm}$ ). The  $^{13}\text{C}$  NMR spectra of HL and **1** show significant downshift ( $\Delta\delta = 44.5\text{ ppm}$ ) of the C-2 atom of phenyl ring (Fig. S6-S7) due to cyclopalladation. Therefore,  $^1\text{H}$  and  $^{13}\text{C}$  NMR spectra of the complex clearly infer that the two thiocarbamoyl groups are equivalent which indicates that the complex formed is symmetrical in nature and is in well agreement with single crystal X-ray diffraction data.



**Scheme 2.** Synthesis of ligand HL (top) and complex **1** (bottom)

## 2.2. Crystal structure of $[PdCl(L)]$ (**1**)

Complex **1** has been crystallized from acetonitrile medium and is found to have space group  $P 2_1 2_1 2_1$  and orthorhombic crystal system. The ORTEP diagram of complex **1** with the atom numbering scheme is shown in Fig. 1a and the three dimensional molecular packing is shown in Fig. 1b. Some important bond lengths and angles are given in Table 1 along with DFT calculated parameters, which show good similitude between them. X-ray crystallographic data reveal that the molecule of  $[PdCl(L)]$  constitutes central Pd atom which is coordinated by two sulfur atoms S1, S2 and one carbon atom C1 of the chelating ligand, whereas the fourth coordination site is satisfied by the terminal Cl atom to form a distorted square plane “S1C1S2Cl”. The coplanar structure renders effective conjugation between the thioamide moieties and the phenyl ring as shown at structure III and V (symmetric) of scheme 1. The observed Pd–S (2.293(3) Å) and Pd–C (1.932(12) Å) distances agree well with the theoretically calculated distances of 2.286 Å and 1.957 Å respectively as well as previously reported values [18,20]. The significantly shorter Pd–C1 bond (1.932(12) Å) [28] than the Pd–C(aryl) bonds (1.98–1.99 Å) of cyclopalladated thiocarboxamide complexes with similar S–C–S donor sets and fused chelate ring system [29] and appreciably long terminal Pd–Cl bond length of 2.445 (3) Å (2.354 Å from DFT analysis) reflecting strong trans-influence [30] which is also consistent with the previous data [12]. The origin of the short Pd–C1 bond may be due to the effective conjugation along the chelate ring and partial double bond character in C1–C6–C13–S2 and C1–C2–C7–S1 which provides a rigid conformation to fit the Pd atom. The terminal chlorine atom is slightly out of the mean coordination plane of the Pd. The deviation of the chlorine atom from the Pd1C1S1S2 plane is 0.338 Å in the crystal structure and 0.007 Å as per DFT calculation. In the crystal lattice, neither intercomponent  $\pi$ -stacking interaction of the centered phenyl ring nor intermolecular  $d^8$ - $d^8$  interaction is

observed with a Pd-Pd distances of 6.573 Å. The C–Pd–Cl is found to be 172.0°(4)) as per the crystal structure and 179.8° according to DFT calculation. The deviation from the linearity in the crystal structure is may be due to the artefact from crystal packing forces.

**Table 1.** Important bond distances and bond angles (Å, °) for (**1**) from X-ray crystallography and DFT

Parameter	X-ray data	DFT	Parameter	X-ray data	DFT
Pd1-S1	2.295(3)	2.285	Pd1-Cl	2.445(3)	2.354
Pd1-S2	2.292(3)	2.286	Pd1-C1	1.932(12)	1.957
S1-Pd1-Cl	93.91(13)	94.55	C1-Pd1-Cl	172.0(4)	179.8
S2-Pd1-S1	169.76(16)	170.7	C7-S1-Pd1	101.2(5)	100.4
S2-Pd1-Cl	95.90(13)	94.75	C13-S2-Pd1	99.4(5)	100.4
C1-Pd1-S1	85.6(4)	85.36	C6-C1-Pd1	122.5(9)	120.8
C1-Pd1-S2	85.1(4)	85.34	C2-C1-Pd1	120.2(9)	120.8

Similar to the previously reported secondary thioamide based pincer complexes, the supramolecular three dimensional crystal structure of **1** consists of intermolecular hydrogen bonding interactions between the hydrogen atoms of carbamoyl, the phenyl ring and t-butyl groups and the terminal chlorine atom indicated as  $H_{\text{carbamoyl}} \cdots \text{Cl}$ ,  $H_{\text{phenyl}} \cdots \text{Cl}$  and  $H_{\text{t-butyl}} \cdots \text{Cl}$  (Table S2, Fig. 1b) [16,21]. These hydrogen-bonding interactions have shown great influence on the overall structural and photophysical properties of this type of compounds [31-32].

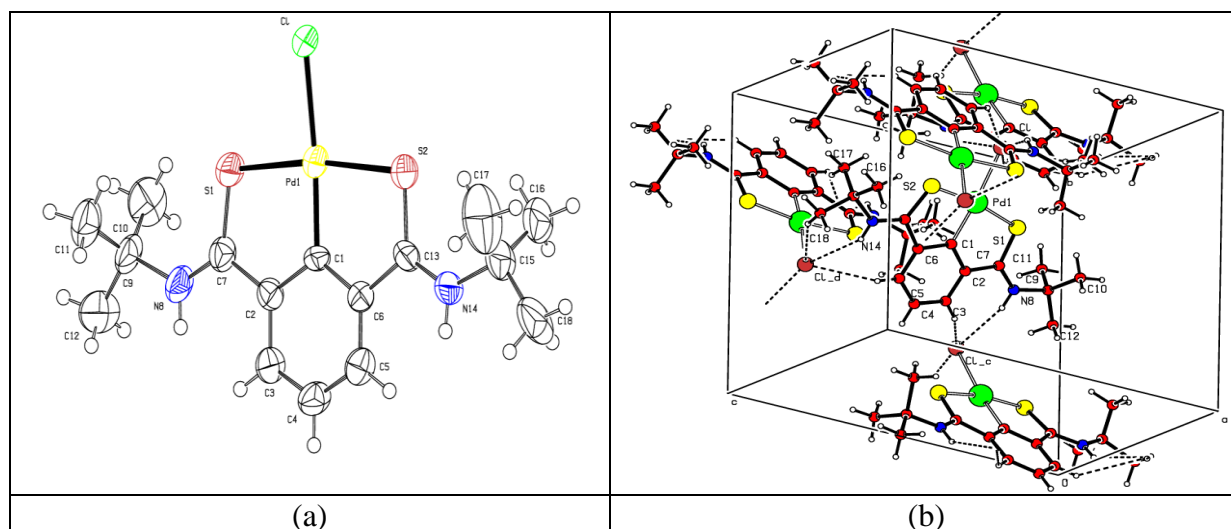


Fig. 1. ORTEP diagram of [PdCl(L)] (**1**) showing the atoms with numbering scheme (displacement ellipsoids are drawn at the 50% probability level) (a) and the three-dimensional structure of **1**, showing all intermolecular hydrogen-bonding interactions constructed by classical N–H···Cl and C–H···Cl interactions (b).

### 2.3. Powder XRD analysis

Powder X-ray diffraction analysis (PXRD) was carried out to confirm the phase purity of the bulk sample of **1** at room temperature (Fig. S8). The experimental diffraction pattern of the bulk sample of **1** is consistent with the corresponding simulated pattern and Bragg position obtained from single crystal X-ray diffraction, indicating that the product formed is pure as present in the single homogeneous phase.

#### 2.4. Photophysical properties

Electronic absorption spectra (Fig. 2) of HL in CH<sub>2</sub>Cl<sub>2</sub>, CH<sub>3</sub>OH, CH<sub>3</sub>CN and DMSO are recorded at room temperature, which showed an intense peak around 282 nm (Table S3 for details) and can be assigned to the  $\pi$ - $\pi^*$  transition located on the aromatic ring (see DFT calculation). The weak absorption peak at around 391 nm corresponds to the n- $\pi^*$  transition originated from the lone pair of electrons of thioamide S-atoms [1,19]. The absorption spectra of complex **1** in CH<sub>3</sub>CN and DMSO showed similar  $\pi$ - $\pi^*$  and n- $\pi^*$  transitions around 325 nm and 373 nm respectively. The  $\pi$ - $\pi^*$  transition is red shifted with respect to the free ligand indicating lowering in energy of the  $\pi^*$  orbital of the aromatic ring because of effective conjugation in the pincer ligand by the cyclopalladation. Apart from these two ligand centered transitions, around 431 nm one additional peak is observed which can be attributed to the spin allowed 4d(Pd) $\rightarrow$  $\pi^*(L)$  (metal-to-ligand charge transfer, MLCT) transition [1,20,33,34] as determined from the DFT based calculation.

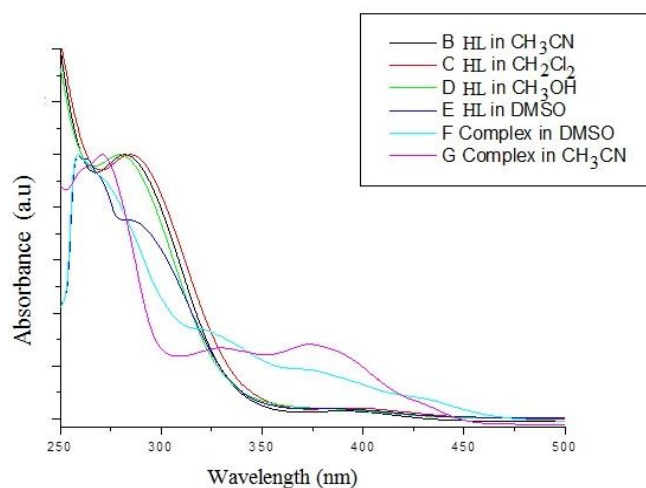


Fig. 2. UV-Visible absorption spectra of HL and complex in different solvent

The UV-Vis absorption spectrum of the ligand in the solid state at 298 K (Fig. S9) displays a broad absorption band consist of ligand centered transitions. The absorption spectrum of the complex is extended up to 850 nm and exhibits a slight bathochromic shift may be due to the bonding and effective conjugation because of cyclometallation of the ligand. This broadness

may be due to the overlapping of ligand centered transitions and spin allowed  $4d(\text{Pd}) \rightarrow \pi^*(\text{L})$  (MLCT) transition within the complex.

By irradiating UV light at 280 nm ( $\lambda_{\text{ex}}$ ), the solid state luminescence spectra are recorded for both ligand and complex at ambient temperature. Ligand showed the main emission peak at around 470 nm with a small peak at 355 nm (Fig. 3). The blue emission at 470 nm can be assigned as ligand centered  $\pi\text{-}\pi^*$  fluorescence transition with an average decay time of 7.1 nsec (fitted by a triexponential decay, Figure S10). The quantum efficiency for this emission was found to be 0.04. On the contrary, neither the ligand nor the complex displayed any emission in the solution of organic solvents like ( $\text{CH}_2\text{Cl}_2$ ,  $\text{CH}_3\text{CN}$ , DMSO) at room temperature similar to the related thioamide and thiophosphoryl based Pd-pincer complexes [1,35]. Exhibition of luminescence at room-temperature by the mononuclear Pd(II) complexes is not very common. Either by blending these type of complexes with suitable organic polymeric matrix or crystallizing in presence of embedded solvent molecules within the crystal structure, the emission can be increased many times [21,32]. Therefore, we have synthesized the complex in pure state which can able to form a three dimensional network through the formation of non-covalent interaction and restrict the molecular distortion. Although **1** doesn't contain any solvent molecule within its crystal structure, it is fairly luminescent at ambient temperature in the solid state (Fig. 3). The emission with maxima at 460 nm is ( $\lambda_{\text{ex}} = 280$  nm) observed with average lifetime of 5.7 nsec (fitted by a triexponential decay, Figure S10), which is in the same range of the decay lifetime of the ligand and can be considered as the ligand centered  $\pi\text{-}\pi^*$  transition in the complex. The fluorescence decay of **1** also follows a triexponential pattern like HL, which may be due to the presence of different canonical structure of the ligand (vide supra). Although most of the pincer palladium complexes show delayed phosphorescence (in the range of msec to  $\mu\text{sec}$  of lifetime) due to significant spin-orbit coupling in these complexes, emission lifetimes in nS range are also reported previously [36,37]. Moreover, although good quantum yield is observed of the similar complexes at low temperature either in the glassy frozen state or in microcrystalline state [20,32], the present study reports comparable quantum yield values at room temperature and in powder form. The quantum yield of **1** is found to be 0.05, slightly more than (0.04) the free ligand. The shifting of this  $\pi\text{-}\pi^*$  transition of **1** with respect to the free ligand HL may be as a result of coordination of the ligand with the metal ion. This type of shifting of  $\pi\text{-}\pi^*$  transition due to metal complexation for a thiophosphoryl-thiocarbamoyl type pincer ligand was also reported by Aleksanyan et al. [2]. Moreover, one additional peak

is observed at 689 nm in case of the complex which is not present for the bare ligand and may be assigned as MLCT transition as reported in earlier studies [20,35]. Therefore, from the luminescence spectra and decay lifetimes of the ligand and the complex it can be inferred that the emission behavior of the complex is mainly originated from the ligand based fluorescence transition with some additional MLCT transition character. The measurable emission from complex **1** indicates that the non-radiative decay pathway such as thermal induced deexcitation is minimum which is not very common for mononuclear Pd-pincer complexes [38].

The luminescence spectra (Fig. S11) of **1** in poly(vinylpyrrolidone) (PVP) matrix at different composition indicate that with decreasing the weight percentage of complex in the matrix the luminescence intensity increases. This clearly signifies that in presence of polymer molecules with H-bond acceptor (carbonyl in the present case), the secondary amide of **1** is chemically bonded to the polymer. This also ruled out the possibility of excimer induced luminescence at higher concentration, when recorded in pure form. This restricts the molecular motion of complex and helps to decrease the non-radiative decay. Similar result is obtained by Ogawa et al. for their palladium based pincer complex blended with polymer matrices and maximum luminescence intensity was observed for 10 wt % complex-PVP hybrid film [21].

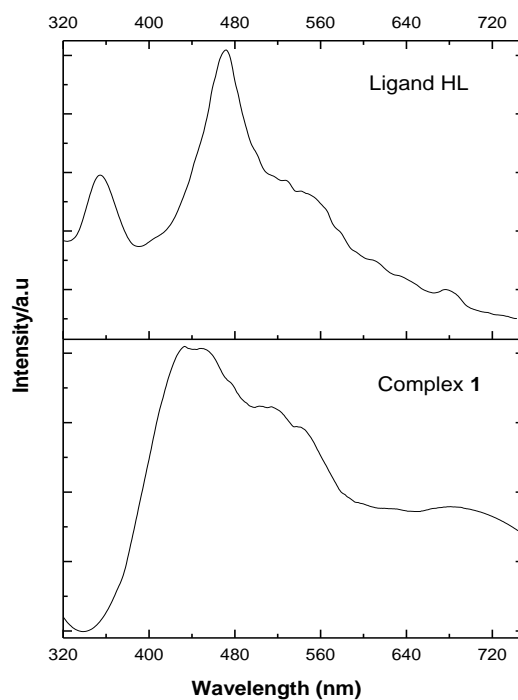


Fig. 3. The luminescence spectra of the ligand (top) and the complex **1** (bottom) in solid state at room temperature (excitation wavelength: 280 nm)

#### 2.4.1 TD-DFT analysis for photophysical studies

To understand the electronic transition of the ligand and the complex in solid state as well as in solution, we have theoretically determined the nature of transition, their oscillation strength and their percentage contribution for the transition. Table 2 shows the details of the calculated results for HL and **1** in acetonitrile medium. A good agreement between the experimental and calculated spectra of the ligand as well as the complex was observed except some additional peaks occurred in the theoretical spectra which may be quenched in solution. Fig. 4 shows some selected frontier molecular orbitals which are related to the transition with high oscillation strength ( $f > 0.01$ ) and low energy electronic transition in case of ligand as well as of complex (isosurface value = 0.05). It can be seen that HOMO-4, LUMO and LUMO+1 of the ligand are localized on aromatic phenyl unit and two attached thioamide groups with  $\pi$  character. The HOMO-2 of the ligand is located on the sulfur atom of the thioamide groups as lone pair of electrons. According to the theoretical calculations, a  $\pi$ - $\pi^*$  transition (HOMO-4 to LUMO+1) at 272 nm and a n- $\pi^*$  transition (HOMO-2 to LUMO) at 373 nm were observed. The strong and weak peaks at 282 and 391 nm respectively in the experimentally observed spectrum are in close agreement with the theoretically predicated transitions. The HOMO-5 and LUMO+1 of the complex **1** are localized on aromatic unit and two attached thioamide groups with  $\pi$  character. The HOMO-4 of **1** is localized on the sulfur atom of the thioamide groups as lone pair of electrons. Based on calculations, a  $\pi$ - $\pi^*$  transition (HOMO-5 to LUMO+1) at 298 nm and a n- $\pi^*$  transition (HOMO-4 to LUMO+1) at 340 nm were observed. The overlapping transition between 325 nm and 373 nm in the experimentally observed spectrum is in close agreement with the theoretically predicated transitions. The both HOMO-1 and HOMO of **1** are mainly composed of d-orbitals ( $d_{x^2-y^2}$ : 33.39 %,  $d_{xy}$ : 11.20 %,  $d_{xz}$ : 1.51 % for HOMO-1 and  $d_{xy}$ : 27.33 %,  $d_{yz}$ : 10.03 %,  $d_{x^2-y^2}$ : 1.19 % for HOMO) of the palladium metal center which indicates the involvement of the metal orbitals in the excitations higher than 400 nm wavelength. Therefore, the transitions at 404 and 443 nm can be assigned as symmetry allowed MLCT transitions [13]. The broad shoulder peak at around 431 nm in the experimental spectrum of the complex relates to the two close lying transitions observed in the theoretical spectrum.

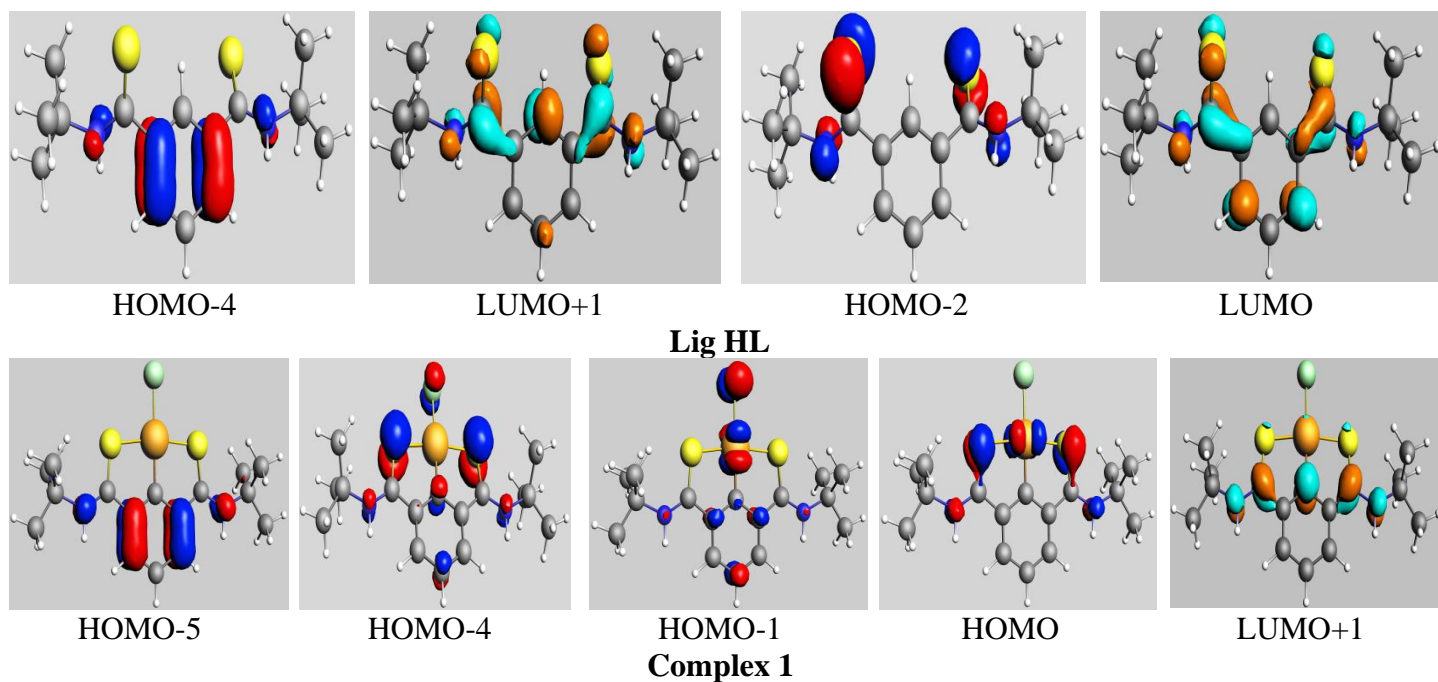


Fig. 4. Frontier molecular orbitals related to the transitions with high oscillation strength ( $f > 0.01$ ) (Color code: Brown: Pd, Yellow: S, Light green: Cl, Grey: C, White: H). Molecular orbitals are obtained at PBE/TZ2P computational level.

**Table 2.** Details of important UV-Vis transitions of HL and **1** in CH<sub>3</sub>CN calculated from DFT

Compound	Calculated transition/nm	Composition	Oscillation strength (f)	Assignment
<b>HL</b>	272	H-4 to L+1 (40.6%)	0.5208	$\pi$ - $\pi^*$
		H-5 to L (12.9%)		
	373	H-2 to L (43.4%)	0.0145	$n$ - $\pi^*$
		H-3 to L (23.4%)		
		H-2 to L+1 (17.9%)		
<b>1</b>	298	H-5 to L+1 (45.7%)	0.4425	$\pi$ - $\pi^*$
		H-4 to L+1 (80.6%)		
	340	H-1 to L+1 (85.2%)	0.1271	MLCT
	404	H to L+1 (72.9%)	0.1787	MLCT

### 2.5. Catalytic activity towards Mizoroki-Heck and Suzuki-Miyaura cross coupling reactions

The catalytic property towards the Mizoroki-Heck reaction has been utilized here for the synthesis of arylated olefins. Several organometallic complexes of palladium bearing hemilabile ligands have been developed as the efficient catalysts towards direct C–C bond construction through different types of cross coupling reaction [39-42]. This is due to the fact that hemilabile ligands facilitate the bonding of the incoming ligand or substrate with the Pd metal center and sometimes support to generate actual catalyst from molecular pre-catalyst [43,44]. Since the structure and reactivity relationship of Pd complexes with thioamide based ligands towards Mizoroki-Heck coupling has been relatively less studied [45], catalytic performances of complex **1** in Mizoroki-Heck reactions of differently substituted bromobenzenes with t-butyl acrylate have been investigated in the present study (Table 3). Also, catalytic efficacy of **1** towards Suzuki-Miyaura coupling reaction with the same set of bromobenzenes and p-tolylboronic acid was studied, and the results are summarized in Table 4. N,N-dimethylformamide (DMF) was used as solvent here for both the reactions, which is very commonly used solvent for these types of reactions. Potassium carbonate ( $K_2CO_3$ ) is chosen as base for these catalytic reactions as it is known to be the most commonly used base [46]. The entries from 1 to 6 show that loading of 0.1 mol % of catalyst can produce good yield (> 90%) of the coupled products in 2 h at 120°C for both the aryl bromides. However, catalyst loadings of less than 0.1 mol % result (entries 3 and 6) much lower yields (~ 53%) even at higher reaction temperature (150°C) and longer reaction time (5 h). Although good catalytic transformation is observed by using complex **1** as catalyst, better reaction yield was found by Lin et al. for bromobenzene using a set of palladium N-heterocyclic carbene complexes [44]. A similar secondary thioamide based palladium pincer complex showed much faster kinetics (only 15 min) when 4-Iodotoluene was reacted with styrene in dimethylacetamide [18]. The yields of coupling product in case of activated aryl halide (electron withdrawing group) i.e. 4-nitro-bromobenzene are always higher than that of the unsubstituted bromobenzene owing to the more favorable oxidative addition (believed to be as an initial step) towards the catalyst by the former substrate. This probably allows to leave the bromide group from the starting material very easily and get attached with the metal atom of the catalyst more efficiently. All the experiments for Suzuki-Miyaura coupling reactions are carried out under the same conditions as that of Mizoroki-Heck reaction i.e., heating in DMF at 120°C using potassium carbonate as a base. Table 4 shows the reaction conditions along with the respective yields of the coupled products. With catalytic loading of 1 mol %

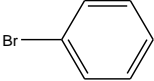
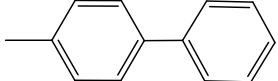
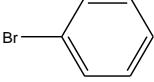
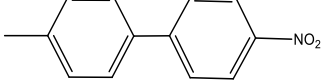
(Entries 1 and 4) and 0.1% (Entries 2 and 5), the corresponding yields of the coupled products are found to be very good (> 96%) with a slight decrease in case of the latter one (> 94%). Catalytic loading of 0.01 mol% produces moderate yield (~ 61%) of the coupling products even at high temperature (150°C) and longer reaction time (5 h). This shows the reaction yield of the cross-coupled products is comparable with other previously reported thioamide and thiophosphoryl mixed palladium pincer complexes [1,2,47,48], although  $K_3PO_4$  rather than  $K_2CO_3$  as base was used and  $Bu_4NBr$  additive was added for these reactions. For the aryl bromide substrates, the normal dependency on the electronic properties of the substituent R (R = H,  $NO_2$ ) was observed. Here also electronically activated 4-nitro-bromobenzene couples more readily than the bromobenzene with the boronic acid.

**Table 3.** Mizoroki–Heck reaction of aryl bromide and t-butyl acrylate

Entry	aryl halide	amount (mol %)	Time (h)	Yield (%)	Product
1		1	2	95.7	
2		0.1	2	93.1	
3		0.01	5	53.3	
4		1	2	99.8	
5		0.1	2	98.1	
6		0.01	5	69.5	

**Table 4.** Suzuki–Miyaura reaction of aryl bromide and p-tolylboronic acid

Entry	aryl halide	amount (mol %)	Time (h)	Yield (%)	Product
1		1	2	96.2	

2		0.1	2	94.6	
3		0.01	5	61.6	
4		1	2	99.6	
5		0.1	2	97.1	
6		0.01	5	73.4	

### 2.5.1 DFT analysis for catalytic studies

Previous studies on the Pd-catalyzed Mizoroki-Heck reaction indicate that two reaction pathways, Pd(0)-Pd(II) and Pd(II)-Pd(IV) [49,50] are possible for the catalytic process. In the former case, the molecular Pd(II)-complex (pre-catalyst) is first reduced to generate activated Pd(0) nanoparticles, which further act as actual catalyst and follow a Pd(0)-Pd(II) pathway through oxidative addition [51-54]. While in the latter case, Pd(II) complex acts as true homogeneous catalyst and get involved in Pd(II)-Pd(IV) pathway by the same oxidative addition method. Keeping this in mind, we have studied both the mechanisms theoretically to trace out the most favourable path for the present case. The catalytic cycles with all intermediates and products are schematically presented in Fig. S12-S16.

In case of Pd(II)-Pd(IV) pathway, the first step i.e., oxidative addition proceeds through the insertion of complex **1** to aryl bromide (Fig. S12). Such insertion leads to a change in coordination number of Pd and its oxidation state to form intermediate **2**. Next, the olefin addition step further strains the coordinating environment of Pd to form the  $\pi$ -complex, a prerequisite for Pd-C<sub>olefin</sub> bond formation. The free energies of these consecutive steps are found to be unfavourable by +27.9 kcal mol<sup>-1</sup> and +11.5 kcal mol<sup>-1</sup>. The highly favourable final reductive elimination step (-100.7 kcal mol<sup>-1</sup>) releases the strain associated with the sterically crowded environment of Pd to yield the desired product. Interestingly, other than this neutral pathway, an alternative pathway involving cationic intermediate PdL<sup>+</sup> is also known. A recent DFT study by Bäcktorp et al. [55] suggests both the approaches are competitive to each other. This pathway requires an initial detachment of Cl<sup>-</sup> from complex **1** in a highly polar solvent (DMF here) to form a positively charged species (**1** in Fig. S13) in order to follow the subsequent reactions. However, in presence of K<sub>2</sub>CO<sub>3</sub> as base, PdL<sup>+</sup> can be deprotonated at one of the two secondary amide sides and form neutral complex PdL

[15,16,18,56-61]. According to our calculation, the free energy of deprotonation of PdL<sup>+</sup> in DMF is found to be -36.7 kcal mol<sup>-1</sup>. This PdL may also have separate catalytic ability although we have not examined this aspect in the present study. In contrary to the neutral pathway, oxidative addition for the cationic reactant changes the coordination number from 3 to 5, which is energetically less demanding (+11.9 kcal mol<sup>-1</sup>) and thus reduces the unfavourability of the first step to an extent of ~16 kcal mol<sup>-1</sup>. Unlike the neutral pathway, starting species **1** in the cationic pathway can participate in oxidative addition to generate three conformational isomers. These isomers differ structurally with respect to the position of aryl and bromide as shown in Fig. S13 (**2a-c**). We have noted that, while **2c** retains its original trigonal bipyramid conformation, **2b** reverts to **2a** during the geometry optimization process. Among these, **2a** is found to be the most stable intermediate and thus it is used for the reaction free energy calculations. Evidently, our DFT investigations suggest that the majority of the involved steps in the Pd(II)-Pd(IV) pathway (both neutral and cationic) are unfavourable and thus diminishes their possibility to emerge as a dominant reaction pathway.

In order to follow the Pd(0)-Pd(II) catalytic cycle, the complex **1** (as pre-catalyst) is to be reduced to elemental Pd(0) (actual catalyst) first. The generation route of elemental Pd is shown in Fig. S14. Complex **1** upon reaction with ArBr first generates hexa-coordinated Pd(IV) intermediate through a transition state. Then a reduced four coordinated intermediate is generated through the release of both the halides in highly polar DMF medium. Next, one intermediate (**4**) is formed in which one of the sulfur atoms get detached from Pd which assist the next reductive elimination process. This type of ligand lability in pincer complexes is shown by Spencer and co-workers although they have investigated the catalytic pathway for Suzuki coupling reaction [62]. It proves that ligand lability in pincer complexes is very supportive and important for catalytic reaction and strengthens our previously mentioned statement. We have investigated the Pd(0)-Pd(II) cycle with two possibilities, one without DMF and another involving DMF (Fig. S15-S16) because of direct or indirect involvement of solvent molecules as evident from the previous reports [63-66]. It is important to note that in the absence of DMF, the oxidative addition occurs at Pd(0) center (d<sup>10</sup> configuration) with no ancillary ligands. Whereas, in presence of two molecules of DMF, an unsaturated 14-electron intermediate as active species (Pd<sup>0</sup>(DMF)<sub>2</sub>) is formed. Further, the presence of DMF as a coordinating ligand ensures the most stable square planar geometry for the intermediates. The major advantage of Pd(0)-Pd(II) cycle is that the destabilizing steric factor (prevalent for intermediates in the aforementioned Pd(II)-Pd(IV) pathway) remains minimal due to the low

coordination number of Pd in all the intermediates. This is evident from the highly favourable reaction free energy values for the oxidative addition, irrespective of the involvement of DMF in the reaction mechanism ( $-22.8 \text{ kcal mol}^{-1}$  and  $-60.9 \text{ kcal mol}^{-1}$  with and without DMF involvement respectively). Considering these aspects, it can be inferred that the Pd(0)-Pd(II) cycle acts as the most possible pathway to result in the catalytic activity of complex **1** towards Mizoroki-Heck reaction.

### **3. Experimental**

#### *3.1. Materials and techniques*

All chemicals are purchased from commercial sources and used as received without further purification. Solvents are distilled by their conventional methods before using. All the syntheses are carried out under nitrogen atmosphere. IR spectra are obtained with a 'JASCO IR-610 spectrophotometer' using a diamond ATR assembly, for the range  $4000\text{-}400 \text{ cm}^{-1}$ . The  $^1\text{H}$  and  $^{13}\text{C}$ -NMR spectra are recorded using either a 'Bruker AMX-200 or 300 spectrometer' at the operating frequencies of 200 and 300 MHz respectively with respect to  $^1\text{H}$ . Chemical analyzes for C, H and N are determined on a 'Elementar vario EL cube analyzer'. Powder XRD of the sample is analyzed with the help of 'Rigaku Mini Flex 600 X-ray diffractometer'. Diffuse reflectance UV-Vis spectra are recorded in the 200-900 nm region, employing a 'JASCO V-670 spectrometer', using  $\text{BaSO}_4$  as a reference material. The steady-state photoluminescence data are recorded on an FS-5 spectrofluorimeter (Edinburgh Instruments, UK). Both the suitable excitation and emission filters are used while measuring the luminescence data. Fluorescence lifetimes (at 467 nm) are measured using a time-correlated single photon counting (TCSPC) set-up from Horiba Scientific (UK). For the present work, a 292 nm diode laser ( $\sim 800 \text{ ps}$ , 1 MHz repetition rate) is used as the excitation source. The goodness of fit is evaluated from the reduced  $\chi^2$  values and visual inspection of the decay and fitted function. Quantum yield of HL and **1** are measured by absolute method using integrating sphere of diameter 15 cm where  $\text{BaSO}_4$  is used as reference material. Absorbed number of photons by the samples is obtained from the difference of diffuse reflectance scan of  $\text{BaSO}_4$  and sample. Finely powdered samples are placed in a quartz sample holder having thickness of 1 mm for recording emission scans. The error in quantum yield values is in the range of 3 to 5%. Luminescence quantum yield ( $\eta$ ) is related to number of photons absorbed ( $\alpha$ ) and number of photons emitted by the sample ( $\epsilon$ ) as,

$$\eta = \frac{\varepsilon}{\alpha} = \frac{\int I_{emission}}{\int I_{ref} - \int I_{sample}}$$

where,  $I_{emission}$  is total area of sample emission spectrum,  $I_{ref}$  is the scattered intensity for  $BaSO_4$ , and  $I_{sample}$  is the scattered intensity for sample. Therefore, difference between areas of  $I_{ref}$  and  $I_{sample}$  will give the photons absorbed by sample.

### 3.2. Crystal structure determination

Crystal data for **1** is measured on an Agilent Super Nova system equipped with a Titan CCD detector at 293(2) K using Cu-K $\alpha$  radiation ( $\lambda = 1.5418 \text{ \AA}$ ). The crystals are positioned 101 mm from the CCD. Data analysis is carried out with the CRYSLIS program [67a]. The structures are solved using direct methods with the SHELXT program [67b]. All non-hydrogen atoms are refined with anisotropic thermal parameters. The hydrogen atoms bonded to carbon atoms are included in the geometric positions and given thermal parameters equivalent to 1.2 times those of the atoms to which they are attached. The structures are refined using SHELXL [67b] refinement package using Least-squares minimization. Selected crystallographic data for **1** is given in Table 5. CCDC 2018422 contains the supplementary crystallographic data for **1**. These data can be obtained free of charge via <http://www.ccdc.cam.ac.uk/conts/retrieving.html>, or from the Cambridge Crystallographic Data Center, 12 Union Road, Cambridge CB2 1EZ, UK; fax: (+44)1223-336-033; or e-mail: [deposit@ccdc.cam.ac.uk](mailto:deposit@ccdc.cam.ac.uk).

**Table 5.** Crystallographic details.

Crystal data	
Chemical formula	[Pd(C <sub>16</sub> H <sub>23</sub> N <sub>2</sub> S <sub>2</sub> )Cl]
$M_r$	449.33
Crystal system, space group	Orthorhombic, $P 2_1 2_1 2_1$
Temperature (K)	293(2)
a,b,c (Å)	9.8233(5), 13.0882(6), 15.2787(6)
$V(\text{\AA}^3)$	1964.38(15)
Z	4
Radiation type	Cu K $\alpha$
$\mu$ (mm <sup>-1</sup> )	10.829
Data collection	
Diffractometer	Supernova
Absorption correction	multi-scan
$T_{min}$ , $T_{max}$	0.01430, 1.00000
No. of measured, independent and	4338, 2960, 2532

observed [ $I > 2\sigma(I)$ ] reflections	
$R_{\text{int}}$	0.057
$\theta_{\text{max}}$ ( $^{\circ}$ )	70.0
Refinement	
$R[F^2 > 2\sigma(F^2)]$ , $wR(F^2)$ , $S$	0.068, 0.177, 1.005
No. of reflections	2960
No. of parameters	205
H-atom treatment	H-atom parameters constrained
$\Delta\rho_{\text{max}}$ , $\Delta\rho_{\text{min}}$ ( $e \text{ \AA}^{-3}$ )	1.087, -0.922

### 3.3. Catalytic activities

#### 3.3.1. General procedures for the Suzuki-Miyaura cross coupling reaction

A mixture of aryl bromide (2.0 mmol), p-tolylboronic acid (0.272 g, 2.0 mmol), the palladium complex **1** (0.01-1 mol %) and potassium carbonate (0.232 g, 4.0 mmol) in dry DMF (2 mL) is refluxed at 120°C for 2 h. Then the solvent is evaporated and the reaction mixture is extracted with diethyl ether. The ether solution is dried over anhydrous sodium sulfate, filtered and passed through a 12" silica column (60–120 mesh). After evaporation of the ether, solid pure products are obtained. The yields of the products obtained from all the reactions are determined after isolation and the products are characterized by  $^1\text{H}$  NMR spectroscopy.

#### 3.3.2. General procedures for the Mizoroki-Heck reaction

A mixture containing aryl bromide (5.0 mmol), t-butyl acrylate (5.0 mmol), the palladium complex **1** (0.01-1 mol %) and potassium carbonate (1.06 g, 10.0 mmol) in dry DMF (2 mL) is refluxed at 120°C for 2 h. After the reaction, the solvent is evaporated. The contents are poured into water, extracted with diethyl ether, dried over  $\text{Na}_2\text{SO}_4$  and passed through a 12" silica column (60–120 mesh). Upon evaporation of the ether, solid pure products are obtained. The yields of the products obtained from all the reactions are determined after isolation and the products are characterized by  $^1\text{H}$  NMR spectra.

#### 3.3.3. Computational details (DFT and TD-DFT)

The geometry of the ligand and complex are optimized in the gas phase by using PBE density functional with def2-TZVP basis set [68] as implemented in TURBOMOLE 6.6 [69] program suite. To get the local minimum energy in the potential energy surface, subsequent analytical frequency calculations are performed. The absence of imaginary vibrational frequencies indicated that the optimized structures are at their potential minima. To determine the excited state energy levels of the ligand and complex time dependent density functional theory (TD-

DFT) calculations are performed with only singlet state energy levels, where PBE functional [70] and TZ2P basis set [71] are used as implemented in ADF 2017 [72]. To obtain absorption spectra of ligand and complex in CH<sub>3</sub>CN, calculations are performed applying COSMO (COnductor-like Screening MOdel) [73] with dielectric constant ( $\epsilon$ ) 37.5.

In order to determine the catalytic pathways of Mizoroki-Heck reactions theoretically, all the starting, intermediate and final products are optimized for geometry using TURBOMOLE 6.6 with PBE functional and TZVP basis set. Tight convergence criterion (energy change  $< 10^{-8}$  Hartree) is opted and analytical frequency calculations are performed to ensure all the structures are stable intermediates with real frequencies. To incorporate the solvent effect in all the calculations, COSMO is applied with DMF as solvent ( $\epsilon = 36.7$ ). Stepwise binding energy for every reaction involved in the probable catalytic pathways of Mizoroki-Heck reaction was mentioned in the supporting information (Fig S12-S16).

### **Conclusion**

In conclusion, cyclometallation reaction of SNS pincer ligand, N,N'-di-tert-butyl-benzene-1,3-dicarbothioamide with lithium tetrachloropalladate(II) results {N,N'-di-tert-butyl-1,3-dicarbothioamide-S,C,S}benzene palladium(II) chloride. The central palladium atom adopts a slightly distorted square planar geometry and surrounded by two sulfur atoms, one carbon and one chlorine atom. The compound showed good catalytic activity towards Suzuki-Miyaura and Mizoroki-Heck cross coupling reactions. The reaction time is relatively less compared to the previously reported thioamide based complexes and the reaction yield is 99.8 % in presence of 1 mol % of catalyst in case of Mizoroki-Heck reaction and 99.6 % for Suzuki-Miyaura reaction. DFT based investigations on the possible reaction mechanism towards Mizoroki-Heck catalysis suggest that Pd(0)-Pd(II) pathway possibly acts as the dominant pathway rather than Pd(II)-Pd(IV) pathway. The prevalent steric effect hinders the oxidative addition steps for Pd(II)-Pd(IV) pathway, where Pd(II) in the complex remains in square planar arrangement. Whereas, Pd(0)-Pd(II) pathway does not involve such sterically strained intermediates makes it a favourable pathway for catalysis reaction and possibly explains the superior performance of complex **1** as a catalyst for Mizoroki-Heck reaction. The compound emits blue light upon excitation of UV light of 280 nm with lifetime of 5.7 nS and quantum yield of 0.05. Therefore this complex could be considered as a luminophore for optical and electroluminescence devices. DFT study indicates the involvement of ligand center and metal to ligand charge transfer type of luminescence in the overall photoluminescence properties of the complex.

**Electronic Supplementary Information available:** Synthetic details, FTIR, NMR spectral data, DFT analysis and X-ray crystallographic details.

### Acknowledgments

Sincere thanks are due to Computer Centre, BARC for providing ANUPAM parallel computational facility. Authors are thankful to Dr. V. Sudarsan, Dr. Nilotpal Barooah, and Dr. Kaustava Bhattacharyya, BARC for their various analytical supports at different stages of study. DD would like to acknowledge Dr. C. P. Kaushik, Shri Anand Gangadharan and Dr. A. S. Pente for their continuous support and encouragement for the work.

### References

- [1] V. A. Kozlov, D. V. Aleksanyan, Y. V. Nelyubina, K. A. Lyssenko, E. I. Gutsul, L. N. Puntus, A. A. Vasil'ev, P. V. Petrovskii, I. L. Odinets, *Organometallics* 27 (2008) 4062-4070.
- [2] D. V. Aleksanyan, V. A. Kozlov, Y. V. Nelyubina, K. A. Lyssenko, L. N. Puntus, E. I. Gutsul, N. E. Shepel, A. A. Vasil'ev, P. V. Petrovskii, I. L. Odinets, *Dalton Trans.* 40 (2011) 1535-1546.
- [3] S. Roy, S. Pramanik, T. Ghorui, K. Pramanik, *RSC Adv.* 5 (2015) 22544-22559.
- [4] Y. Nojima, M. Nonoyama, K. Nakajima, *Polyhedron* 15 (1996) 3795-3809.
- [5] T. G. Grinter, D. Leaver, R. M. O'Neil, *Inorg. Nucl. Chem. Lett.* 16 (1980) 145-147.
- [6] S. Takahashi, M. Nonoyama, M. Kita, *Transit. Met. Chem.* 20 (1995) 528-532.
- [7] D. C. Marelius, E. H. Darrow, C. E. Moore, J. A. Golen, A. L. Rheingold, D. B. Grotjahn, *Chem. Eur. J.* 21 (2015) 10988-10992.
- [8] K. Yamamoto, K. Higuchi, M. Ogawa, H. Sogawa, S. Kuwata, Y. Hayashi, S. Kawauchi, T. Takata, *Chem. Asian J.* 15 (2020) 356-359.
- [9] S. Das, V. Subramanian, G. Mani, *Inorg. Chem.* 58 (2019) 3444-3456.
- [10] K. Takenaka, M. Minakawa, Y. Uozumi, *J. Am. Chem. Soc.* 127 (2005) 12273-12281.
- [11] Z. Wang, Z. Sun, X. -Q. Hao, J. -L. Niu, D. Wei, T. Tu, J. -F. Gong, M. -P. Song, *Organometallics* 33 (2014) 1563-1573.
- [12] A. R. Naziruddin, C. -S. Lee, W. -J. Lin, B. -J. Sun, K. -H. Chao, A. H. H. Chang, W. -S. Hwang, *Dalton Trans.* 45 (2016) 5848-5859.
- [13] J. Kuwabara, G. Munezawa, K. Okamoto, T. Kanbara, *Dalton Trans.* 39 (2010) 6255-6261.

- [14] D. V. Aleksanyan, Z. S. Klemenkova, A. A. Vasil'ev, A. Y. Gorenberg, Y. V. Nelyubina, V. A. Kozlov, *Dalton Trans.* 44 (2015) 3216-3226.
- [15] T. Suzuki, Y. Kajita, H. Masuda, *Dalton Trans.* 43 (2014) 9732-9739.
- [16] K. Okamoto, J. Kuwabara, T. Kanbara, *Chem. Lett.* 44 (2015) 102-110.
- [17] T. Murai, "Chemistry of Thioamides", Springer (2019).
- [18] R. A. Begum, D. Powell, K. Bowman-James, *Inorg. Chem.* 45 (2006) 964-966.
- [19] K. Okamoto, T. Kanbara, T. Yamamoto, A. Wada, *Organometallics* 25 (2006) 4026-4029.
- [20] M. Akaiwa, T. Kanbara, H. Fukumoto, T. Yamamoto, *J. Organomet. Chem.* 690 (2005) 4192-4196.
- [21] Y. Ogawa, A. Taketoshi, J. Kuwabara, K. Okamoto, T. Fukuda, T. Kanbara, *Chem. Lett.* 39 (2010) 385-387.
- [22] M. A. Hossain, S. Lucarini, D. Powell, K. Bowman-James, *Inorg. Chem.* 43 (2004) 7275-7277.
- [23] P. Pattanayak, J. L. Pratihari, D. Patra, P. Brandão, V. Felix, S. Chattopadhyay, *Polyhedron* 79 (2014) 43-51.
- [24] M. Neumeyer, R. Brückner, *Angew. Chem. Int. Ed.* 56 (2017) 3383-3388.
- [25] R. Lambert, A. L. Wirotius, J. Vignolle, D. Taton, *Polym. Chem.* 10 (2019) 460-466.
- [26] S. -Y. Liu, H. -Y. Li, M. -M. Shi, H. Jiang, X. -L. Hu, W. -Q. Li, L. Fu, H. -Z. Chen, *Macromolecules* 45 (2012) 9004-9009.
- [27] S. Scheibye, B. S. Pedersen, S. O. Lawesson, *Bull. Soc. Chim. Belg.* 87 (1978) 229-238.
- [28] A. G. Orpen, L. Brammer, F. H. Allen, O. Kennard, D. G. Watson, R. Taylor, *J. Chem. Soc. Dalton Trans.* (1989) S1-S83.
- [29] J. E. Kickham, S. J. Loeb, *Inorg. Chem.* 33 (1994) 4351-4359.
- [30] T. G. Appleton, H. C. Clark, L. E. Manzer, *Coord. Chem. Rev.* 10 (1973) 335-422.
- [31] K. Okamoto, T. Yamamoto, T. Kanbara, *J. Nanosci. Nanotechnol.* 9 (2009) 646-649.
- [32] J. Kuwabara, Y. Ogawa, A. Taketoshi, T. Kanbara, *J. Organomet. Chem.* 696 (2011) 1289-1293.
- [33] S. -W. Lai, T. -C. Cheung, M. C. W. Chan., K. -K. Cheung, S. -M. Peng, C. -M. Che, *Inorg. Chem.* 39 (2000) 255-262.
- [34] T. Kanbara, T. Yamamoto, *J. Organomet. Chem.* 688 (2003) 15-19.
- [35] J. Kuwabara, T. Kanbara, *J. Photopolym. Sci. Technol.* 21 (2008) 349-353.

- [36] N. Bandyopadhyay, A. B. Pradhan, S. Das, L. Lu, M. Zhub, S. Chowdhury, J. P. Naskar, *J. Photochem. Photobio. B* 160 (2016) 336-346.
- [37] F. -F. Hung, S. -X. Wu, W. -P. To, W. -L. Kwong, X. Guan, W. Lu, K. -H. Low, C. -M. Che, *Chem. Asian J.* 12 (2017) 145-158.
- [38] F. Neve, A. Crispini, C. D. Pietro, S. Campagna, *Organometallics* 21 (2002) 3511-3518.
- [39] I. P. Beletskaya, A. V. Cheprakov, *Chem. Rev.* 100 (2000) 3009-3066.
- [40] W. Cabri, I. Candiani, *Acc. Chem. Res.* 28 (1995) 2-7.
- [41] F. Alonso, I. P. Beletskaya, M. Yus, *Tetrahedron* 61 (2005) 11771-11835.
- [42] J. -P. Corbet, G. Mignani, *Chem. Rev.* 106 (2006) 2651-2710.
- [43] C. Valente, S. Çalimsiz, K. H. Hoi, D. Mallik, M. Sayah, M. G. Organ, *Angew. Chem. Int. Ed.* 51 (2012) 3314-3332.
- [44] Y. C. Lin, H. H. Hsueh, S. Kanne, L. K. Chang, F. C. Liu, I. J. B. Lin, G. H. Lee, S. M. Peng, *Organometallics* 32 (2013) 3859-3869.
- [45] E. C. Keske, O. V. Zenkina, R. Wang, C. M. Crudden, *Organometallics* 31 (2012) 6215-6221.
- [46] W. -H. Yang, C. -S. Lee, S. Pal, Y. -N. Chen, W. -S. Hwang, I. J. B. Lin, J. -C. Wang, *J. Organomet. Chem.* 693 (2008) 3729-3740.
- [47] V. A. Kozlov, D. V. Aleksanyan, A. A. Vasil'ev, I. L. Odinetz, *Phosphorus Sulfur Silicon Relat. Elem.* 186 (2011) 626-637.
- [48] V. A. Kozlov, D. V. Aleksanyan, Y. V. Nelyubina, K. A. Lyssenko, A. A. Vasil'ev, P. V. Petrovskii, I. L. Odinetz, *Organometallics* 29 (2010) 2054-2062.
- [49] P. W. V. Böhm, W. A. Herrmann, *Chem. Eur. J.* 7 (2001) 4191-4197.
- [50] S. Crestina, S. Consorti, F. R. Flores, J. Dupont, *J. Am. Chem. Soc.* 127 (2005) 12054-12065.
- [51] S. S. Zalesskiy, V. P. Ananikov, *Organometallics* 31 (2012) 2302-2309.
- [52] R. Narayanan, M. A. El-Sayed, *J. Am. Chem. Soc.* 125 (2003) 8340-8347.
- [53] E. H. Rahim, F. S. Kamounah, J. Frederiksen, J. B. Christensen, *Nano Lett.* 1 (2001) 499-501.
- [54] F. Habib, I. Nasser, G. Arash, G. Maryam, H. S. Jafar, *Bull. Chem. Soc. Jpn.* 84 (2011) 100-109.
- [55] C. Bäcktorp, P. O. Norrby, *Dalton Trans.* 40 (2011) 11308-11314.
- [56] H. Wang, J. Liu, Y. Deng, T. Min, G. Yu, X. Wu, Z. Yang, A. Lei, *Chem. Eur. J.* 15 (2009) 1499-1507.

- [57] Q. -Q. Wang, R. A. Begum, V. W. Day, K. B. -James, *Inorg. Chem.* 51 (2012) 760-762.
- [58] J. Liu, H. Wang, H. Zhang, X. Wu, H. Zhang, Y. Deng, Z. Yang, A. Lei, *Chem. Eur. J.* 15 (2009) 4437-4445.
- [59] H. Zhang, A. Lei, *Dalton Trans.* 40 (2011) 8745-8754.
- [60] I. L. Odinets, D. V. Aleksanyan, V. A. Kozlov, *Lett. Org. Chem.* 7 (2010) 583-595.
- [61] D. V. Aleksanyan, S. G. Churusova, Z. S. Klemenkova, Y. V. Nelyubina, A. S. Peregudov, V. A. Kozlov, *J. Organomet. Chem.* 886 (2019) 40-47.
- [62] S. Boonseng, G. W. Roffe, M. Targema, J. Spencer, H. Cox, *J. Organomet. Chem.* 845 (2017) 71-81.
- [63] J. Sherwood, J. H. Clark, I. J. Fairlamb, J. M. Slattery, *Green Chem.* 21 (2019) 2164-2213.
- [64] H. Yano, Y. Nakajima, Y. Obora, *J. Organomet. Chem.* 745 (2013) 258-261.
- [65] S. Asada, A. Nito, Y. Miyagi, J. Ishida, Y. Obora, F. Sanda, *Macromolecules* 50 (2017) 4083-4087.
- [66] J. A. Molina de la Torre, P. Espinet, A. C. Albeniz, *Organometallics* 32 (2013) 5428-5434.
- [67] (a) Oxford Diffraction Ltd, CRYCALIS, Oxford Diffraction Ltd, Abingdon, U. K., 2006; (b) G.M. Sheldrick, *Acta Cryst. A* 71 (2015) 3-8.
- [68] A. Schäfer, C. Huber, R. Ahlrichs, *J. Chem. Phys.* 100 (1994) 5829-5835.
- [69] R. Ahlrichs, M. K. Armbruster, R. A. Bachorz, M. Bär, H. P. Baron, R. Bauernschmitt, F. A. Bischoff, S. Böcker, N. Crawford, P. Deglmann, F. Della Sala, TURBOMOLE 6.6, a development of University of Karlsruhe and Forschungszentrum Karlsruhe GmbH; TURBOMOLE GmbH: Jena, Germany, (2014) 1989-2007.
- [70] J. P. Perdew, K. Burke, M. Ernzerhof, *Phys. Rev. Lett.* 77 (1996) 3865-3868.
- [71] E. V. Lenthe, E. J. Baerends, *J. Comput. Chem.* 24 (2003) 1142-1156.
- [72] G. teVelde, F. M. Bickelhaupt, E. J. Baerends, C. Fonseca Guerra, S. J. A. van Gisbergen, J. G. Snijders, T. Ziegler, *J. Comput. Chem.* 22 (2001) 931-967.
- [73] A. Klamt, G. Schuurmann, *J. Chem. Soc. Perkin Trans. 2* (1993) 799-805.